Chiral superfluidity of helium-3 in the quasi-two-dimensional limit

Petri J. Heikkinen,* Lev V. Levitin, Xavier Rojas, Angadjit Singh,† Nathan Eng, Andrew Casey, and John Saunders‡
Department of Physics, Royal Holloway, University of London, Egham TW20 0EX, Surrey, United Kingdom

Anton Vorontsov
Department of Physics, Montana State University, Bozeman, Montana 59717, USA

Nikolay Zhelev,§ Abhilash Thanniyil Sebastian,¶ and Jeevak M. Parpia
Department of Physics, Cornell University, Ithaca, New York 14853, USA
(Dated: September 20, 2024)

Anisotropic pair breaking close to surfaces favors chiral superfluid ^{3}He-A over time-reversal invariant ^{3}He-B. Confining superfluid ^{3}He into a cavity of height D of the order of the Cooper pair size characterized by the coherence length ξ_0—ranging between 16 nm (34 bar) and 77 nm (0 bar)—extends the surface effects over the whole sample volume, thus allowing stabilization of the A phase at pressures P and temperatures T where otherwise the B phase would be stable. In this work the surfaces of such a confined sample are covered with a superfluid ^{4}He film to create specular quasiparticle scattering boundary conditions, preventing the suppression of the superfluid order parameter. We show that the chiral A phase is the stable superfluid phase under strong confinement over the full $P-T$ phase diagram down to a quasi-two-dimensional limit $D/\xi_0 = 1$. The planar phase, which is degenerate with the chiral A phase in the weak-coupling limit, is not observed. The gap inferred from measurements over the wide pressure range from 0.2 to 21.0 bar leads to an empirical ansatz for temperature-dependent strong-coupling effects. We discuss how these results pave the way for the realization of the fully-gapped two-dimensional $p_x + ip_y$ superfluid under more extreme confinement.

Chiral superconductivity is a rare phenomenon with non-trivial topology, predicted to result in several exotic properties [1]: macroscopic angular momentum [2–4]; anomalous quantum Hall effect [2, 5, 6]; half-quantum vortices [7–10]; spontaneous chiral edge currents [4, 11]; and chiral Majorana states bound on the edges and vortex cores [6, 10, 12–15], obeying non-Abelian braiding statistics required for topological quantum computation [16–19]. Various superconducting materials have been proposed to realize chiral Cooper pairing [20, 21], e.g., Sr_2RuO_4 [22–24], UPt_3 [25–28], UTe_2 [29], $LaPt_3P$ [30], $SrPtAs$ [31, 32], and URu_2Si_2 [33]. Although most of these materials show evidence for broken time-reversal symmetry, the actual pairing states are still under debate [1, 20, 21]. Conversely, the unconventional p-wave spin-triplet pairing in superfluid helium-3 is well-established [34–36], with one of its stable phases, ^{3}He-A, having a directly measurable chirality [37–40]. Importantly, the coherent nuclear dipole interactions, determining the weak spin-orbit coupling in superfluid ^{3}He, allow the interrogation of the nuclear spins of the paired ^{3}He fermions directly by nuclear magnetic resonance (NMR) to determine the order parameter.

Bulk ^{3}He is distinguished from its metal counterparts by the maximal symmetry group $SO(3)_L \times SO(3)_S \times U(1)_\phi \times T \times C \times P$ of the normal state [35, 41]. Here $SO(3)_L$ and $SO(3)_S$ denote the three-dimensional rotations in the orbital and spin spaces, respectively, and $U(1)_\phi$ is the gauge symmetry. These continuous symmetry groups are combined with the time-reversal (T), particle-hole (C), and parity (P) discrete symmetries.

Consequently, the irreducible representations from which the order parameter is constructed are simple spherical harmonics of degree one. In the bulk liquid at zero magnetic field there are two stable phases with distinct broken symmetries: chiral A phase with point nodes in the energy gap and time-reversal-invariant B phase with isotropic gap. ^{3}He-B dominates the $P-T$ phase diagram with the chiral ^{3}He-A restricted to temperatures relatively close to the bulk superfluid transition temperature T_{c0} at pressures above the polycritical point at $P_c = 21.22$ bar, see Fig. 1a [35].

In this work we explore the effect of very strong anisotropic confinement on the superfluid. This breaks its rotational symmetries, leading to the predicted stability of the chiral A phase over the entire $P-T$ phase diagram [42–47]. Confinement in the absence of disorder is achieved in a nanofabricated slab geometry of height $D = 80$ nm, which is comparable to the zero-temperature coherence length $\xi_0 = \hbar v_F / 2\pi k_B T_{c0}$ and approaches the quasi-two-dimensional limit $D/\xi_0 = 1$ at low pressures. Here v_F is the Fermi velocity. The observed order-parameter suppression arising from pair breaking by surface scattering [42, 48–51], which we tune to be specular, is minimal [47]. As a consequence, access is opened to even stronger confinement in which the size quantization across the sample can play a significant role. This potentially leads to a fully gapped two-dimensional chiral ^{3}He-A. The absence of gap nodes in the pure 2D case eliminates the nodal low-energy quasiparticles, leaving Majorana-Weyl edge states as the only available sub-gap states. Moreover, tuning the cavity

height is predicted to lead to analogues of the quantum Hall effect [2, 5, 34].

An important consideration is the relative stability of the chiral A phase and the time-reversal-invariant planar phase (2D helical phase), particularly at low pressures, since these phases are degenerate in the weak-coupling limit [35]. However, in our experiment we found no evidence of any phase other than the A phase. This discovery does not support the interpretation of a transport anomaly observed at a film thickness $D = 137$ nm in terms of a phase transition from ^{3}He-A into a different phase [52]. Furthermore, having access to the A phase over a wide temperature and pressure range, we characterized the pressure and temperature dependence of the strong-coupling effects stabilizing it.

We report SQUID-amplified NMR experiments performed using the setup described in Refs. [46, 47, 53, 54]. The sample container with atomically smooth walls (0.1 nm surface roughness) was nanofabricated out of two silicon pieces. The silicon patterning process followed Refs. [55, 56]; an additional step of thermal oxidation passivated the surfaces [57, 58] before fusion bonding the patterned wafer and the lid together [54]. The cavity was connected to the fill line by a set of five 2.5 mm × 10 µm × 50 µm trenches [54] providing the "bulk marker" for in situ determination of T_{c0} [47]. We performed NMR in a magnetic field of approximately 30 mT perpendicular to the cavity, $\mathbf{H}_0 \parallel \hat{\mathbf{z}}$, corresponding to the Larmor frequency $f_L = 1005$ kHz. Magnetic field gradients were applied to separate the signals arising from the cavity and the bulk marker, and to suppress the signal from the mouth of the fill line.

The temperature of the heat exchanger was measured with a Pt-NMR thermometer, calibrated against the ^{3}He melting curve [67]; the temperature gradient between the helium in the cavity and the Pt sensor was inferred as described in the Supplementary Information of Ref. [47].

To achieve essentially specular quasiparticle scattering at the boundaries [46, 47, 68, 69], we preplated the surfaces with 100 µmol/m^2 of ^{4}He prior to filling the cell with ^{3}He. For this preplating the temperature gradient across the cavity and the bulk marker is negligible [47].

The phase diagram was mapped with NMR pulses with a small tipping angle $\beta < 10°$, applied while ramping the temperature up or down at a rate of 10–30 µK/hour, see Fig. 2a. The superfluidity manifests as an NMR precession frequency shift $\Delta f = f - f_L$ away from the Larmor frequency, with an onset at the superfluid transition temperature T_c. The minute suppression of T_c with respect to the bulk marker transition temperature T_{c0}, Fig. 1c, indicates that the surface scattering is nearly perfectly specular. Within the quasiclassical theory [45, 51, 70] this can be parameterized in terms of specularity S, the probability of specular scattering [47, 50]. Our data correspond to $S > 0.97$ over the entire pressure range, consistent with T_c suppression measured in a $D = 192$ nm
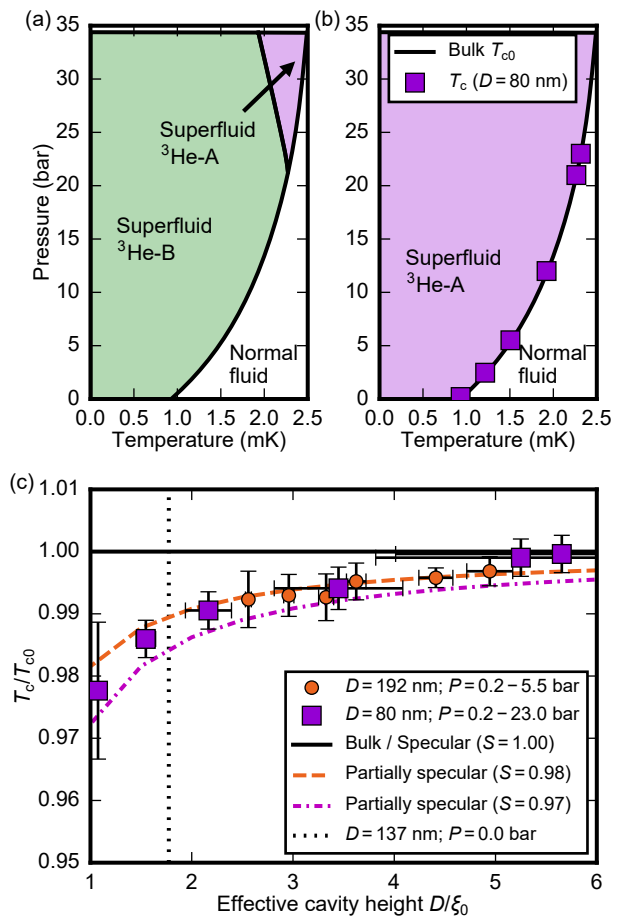

FIG. 1. (Color online) Phase diagrams of bulk ^{3}He with two superfluid phases (a) and of ^{3}He in the $D = 80$ nm cavity, where ^{3}He-A is the only stable superfluid phase (b). The pressures covered in this work were 0.2, 2.5, 5.5, 12.0, 21.0, and 23.0 bar (*violet squares*). (c) The suppression of superfluid transition temperature T_c/T_{c0} by confinement against the effective cavity height D/ξ_0 driven with geometry and pressure, with smaller values of D/ξ_0 corresponding to lower pressures. These universal coordinates demonstrate good agreement with the measurements in the $D = 192$ nm cavity with similar ^{4}He preplating (*orange circles*) [47]. The suppression of T_c is extremely small, consistent with calculated specularity $S > 0.97$ (*dash-dotted line*). The horizontal error bars encompass the cavity height distortion induced by pressure (maximally 2.6 nm/bar), as estimated from a finite-element model [47]. The *vertical dotted line* denotes the transport anomaly reported in a ^{3}He film at $D = 137$ nm at 0 bar [52].

cavity [47]. The calculations using quasiclassical theory demonstrate that in the case of the A phase the $S = 0.98$ surface specularity reduces the energy gap in a $D = 80$ nm cavity only by 2.5–5.0% at 0.2 bar and by 0.5–1.0% at 21.0 bar with respect to the bulk gap achieved for $S = 1.0$ [59]. Thus we directly use the magnitude of the measured frequency shift, proportional to the square of the energy gap, to identify the confined superfluid as
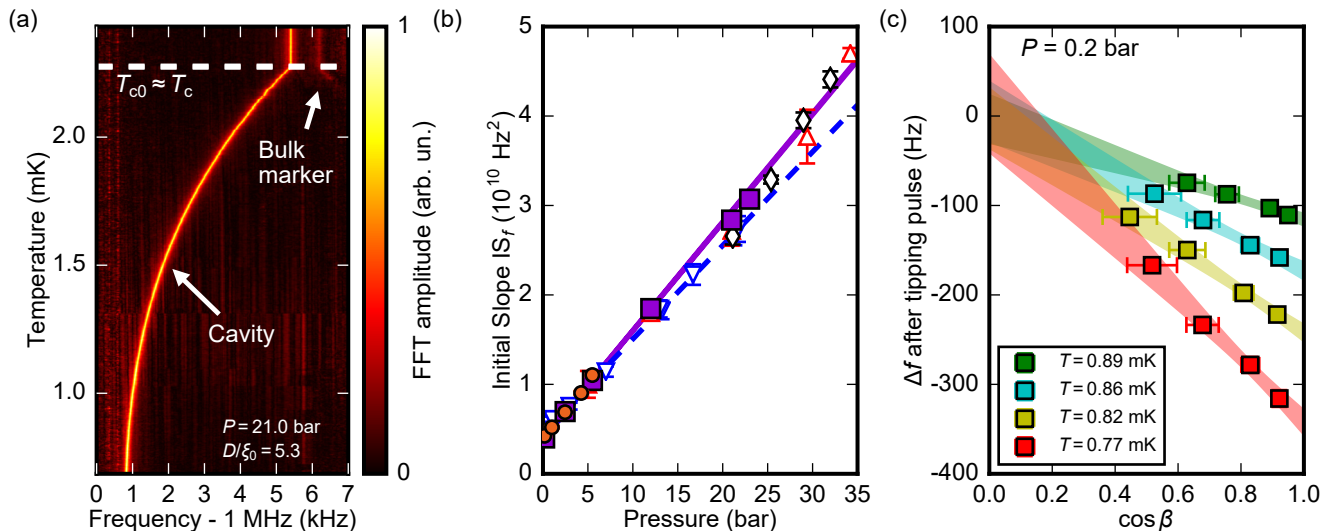
FIG. 2. (Color online) NMR signatures of the superfluidity in the 80 nm high slab-shaped cavity. (a) Colormap of NMR spectra arising from the cavity and the bulk marker as a function of temperature at 21.0 bar. The cavity signal has a constant magnitude and negative frequency shift below the superfluid transition temperature T_c, characteristic of the ^{3}He-A with dipole-unlocked spin-orbit orientation. The bulk marker, shifted to higher normal-state frequency by a magnetic field gradient, shows the expected positive frequency shift below the bulk superfluid transition temperature T_{c0} and is lost on cooling due to broadening. *White dashed line* indicates the measured superfluid transition temperatures in the cavity and in the bulk marker, which at $P = 21.0$ bar are virtually equal (see Fig. 1c). (b) The initial slope of the frequency shift in the cavity in comparison with prior measurements in the A phase. Closed symbols mark the values determined by us under confinement with the specular boundary condition: $D = 80$ nm (*violet squares*) and $D = 192$ nm (*orange circles*) [47]. The *violet line* is a linear fit to these combined data sets [59]. The high-field experiments (*blue downward-pointing triangles*) and the linear fit (*blue dashed line*) of the bulk ^{3}He-A initial slope are from Refs. [60–62]. The data based on stable or supercooled bulk ^{3}He-A are from Ref. [63] (*red upward-pointing triangles*) and Ref. [64] (*black diamonds*). To compensate for the systematic differences arising from different definitions of IS$_f$, small adjustments have been made to some of the values [47, 59]. (c) The dependence of the cavity frequency shift Δf on the tipping angle β is consistent with $\Delta f(\beta) \propto -\cos\beta$ (*colored bands*), a signature of the A phase with $\hat{\mathbf{d}} \perp \hat{\mathbf{l}} \parallel \mathbf{H}_0$. The range of β was limited to $\beta < 60°$ by anomalous NMR heating of confined helium [65]. To mitigate the effect the measurements employed the "pulse-antipulse" technique to vary β at a constant level of heating [66]. The legend quotes the temperature of confined helium inferred from $\Delta f(\beta \to 0)$ (based on data in Fig. 3).

the A phase close to T_c and to measure the bulk A-phase gap over a wide temperature and pressure range.

The temperature-independent magnitude of the cavity signal (constant sample magnetization), as exemplified in Fig. 2a, indicates equal spin pairing, consistent with ^{3}He-A. The superfluid frequency shift Δf is negative, as expected for the dipole-unlocked spin-orbit orientation of the A phase, previously identified in less confined systems [43, 46, 64, 68]. This orientation is characterized by mutually perpendicular orbital angular momentum $\hat{\mathbf{l}}$ and zero-spin direction $\hat{\mathbf{d}}$, with the former locked perpendicular to the surface throughout the cavity by the strong confinement and the latter perpendicular to the magnetic field. At small tipping angles ($\cos\beta \approx 1$) the frequency shift in this orientation is of the same magnitude and opposite sign as in the bulk. To confirm this, the initial slope IS$_f = \partial |f^2 - f_L^2| / \partial (1 - T/T_c)$ of the measured frequency shift is in good agreement with the prior A-phase measurements, Fig. 2b. In this work we determine the initial slopes over the $0.90 T_c < T < T_c$ temperature

range where the frequency shift is still expected to vary linearly with temperature [47, 59]. Further verification of the A phase with $\hat{\mathbf{d}} \perp \hat{\mathbf{l}} \parallel \mathbf{H}_0$ is the tipping-angle dependence $\Delta f(\beta) \propto -\cos\beta$ [43], Fig. 2c.

We now review the NMR signatures of the planar phase, the strongest (and, to our knowledge, the only) alternative candidate for the superfluid state in our cavity consistent with the temperature-independent magnetization. Since the planar phase is the extreme limit of the B phase with planar distortion [46, 65, 66], two nonequivalent spin-orbit orientations can be realized in a cavity with magnetic field normal to it. We readily rule out the stable orientation P$_+$ characterized by $\Delta f > 0$. However, in the metastable P$_-$ state Δf has the same sign and tipping-angle dependence as the dipole-unlocked A phase in our geometry. Moreover, its magnitude coincides with that of the A phase in the weak-coupling limit, making it difficult to distinguish these phases from the NMR signatures alone. However, below a critical magnetic field of order the dipole field $H_D \sim 3$ mT [35] P$_-$
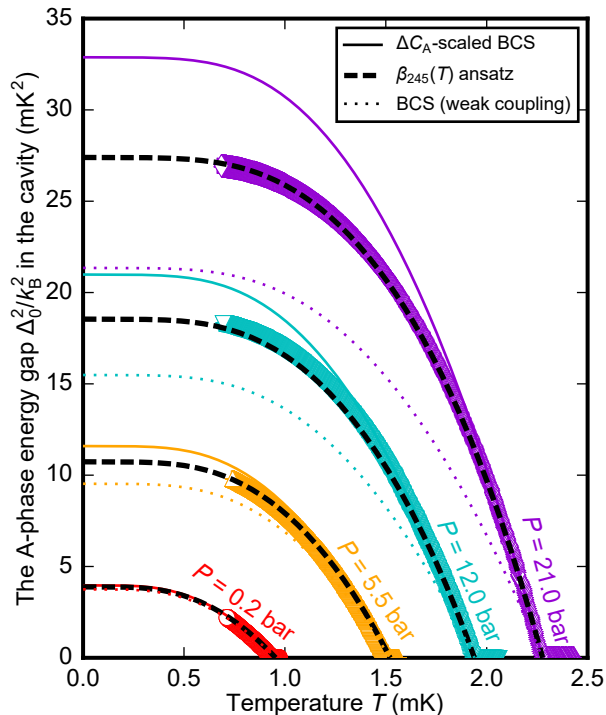
FIG. 3. (Color online) The temperature dependence of the A-phase energy gap Δ_0^2/k_B^2 inferred from NMR using Eq. (1) (*open symbols*) in comparison with various theoretical models. The pressure (*color coded*) tunes the strong-coupling effects. The BCS gap (*dotted lines*), fully determined by T_{c0}, undershoots the data. Near T_{c0} the agreement is improved by scaling the BCS gap using Eq. (2) with experimentally determined β_{245} [71] (*solid lines*). The ansatz, Eq. (3), for the temperature dependence of β_{245} describes the measured gap over the full temperature range (*dashed lines*). One more pressure is shown in the Supplemental Material [59].

becomes unstable and converts into P_+ [65]. Thus, we ruled out the planar phase by observing no change to the negative frequency shift upon cycling the magnetic field down to zero and back up [59].

Figure 3 shows the A-phase energy gap inferred from the small-tipping-angle frequency shift via pressure-dependent temperature-independent scaling [47]

$$\Delta_0^2(T) = \frac{IS_\Delta}{IS_f}\left|f^2(T) - f_L^2\right|. \qquad (1)$$

Here Δ_0 refers to the maximum A-phase energy gap in the momentum space at $\hat{\mathbf{p}} \perp \hat{\mathbf{l}}$. The initial slope of the gap $IS_\Delta = \partial \Delta_0^2/\partial(1 - T/T_{c0}) \propto \Delta C_A \propto 1/\beta_{245}$ is directly related to the A-phase heat capacity jump ΔC_A at T_{c0}, which is inversely proportional to the Ginzburg-Landau parameter β_{245} [35, 71].

The data clearly deviate from the weak-coupling gap $\Delta_{0,BCS}(T)$ obtained within the p-wave Bardeen-Cooper-Schrieffer (BCS) theory. This is a manifestation of

strong-coupling effects, particularly prominent at high pressures [70]. Agreement near T_{c0} can be achieved by scaling the BCS gap [47] by the ratio of the β_{245}^{BCS} obtained from the BCS theory and β_{245} derived experimentally at a given pressure [71]:

$$\Delta_0^2(T) = \frac{\beta_{245}^{BCS}}{\beta_{245}}\Delta_{0,BCS}^2(T). \qquad (2)$$

However, Eq. (2) overestimates the data at low temperatures and high pressures. This is consistent with the reduction of the strong-coupling effects on cooling, which has been incorporated into Ginzburg-Landau theory in terms of temperature-dependent β_i parameters [72]. We introduce an ansatz for this temperature dependence [59]:

$$\beta_{245}(T) = \beta_{245}^{BCS} + \left(\beta_{245}(T_{c0}) - \beta_{245}^{BCS}\right)$$
$$\times \left(1 - 0.09\frac{\Delta_{0,BCS}^2(T)}{k_B^2 T_{c0}^2}\right), \qquad (3)$$

where $\beta_{245}(T_{c0}) \equiv \beta_{245}$ is the conventional Ginzburg-Landau parameter measured near T_{c0} [71]. Substituting Eq. (3) into Eq. (2) leads to excellent agreement with the experimental data over the full temperature and pressure range. We propose that Eq. (3) and similar expressions for the other β_i parameters may improve the quantitative predictions of the Ginzburg-Landau theory at low temperatures.

In conclusion, the constant signal magnitude, as well as the sign, tipping-angle dependence, and the initial slope of the frequency shift Δf very strongly suggest that the chiral ^{3}He-A is the only stable superfluid phase under strong confinement down to $D/\xi_0 = 1$. The earlier observation of a discontinuity in the superfluid density as a function of film thickness at $D = 137\,$nm was obtained using a torsional oscillator with a mechanically polished, but still relatively rough, Cu disk as the substrate for the ^{3}He film [52]. Thus the observed transport anomaly possibly reflects a change in film morphology, with extra superflow paths in thicker films. In contrast to our experiment, the boundaries of this film were a free surface and the solid ^{3}He boundary layer, which we subsequently have found to influence the surface quasiparticle scattering [47]. Determination of the order parameter in this case is a goal of future work.

The possibility to create nearly perfectly specular surfaces by ^{4}He preplating provides the mechanism to observe unsuppressed superfluidity in thin films. This will enable future investigations deeper into the two-dimensional regime $D/\xi_0 < 1$ [73]. Treating a thin helium film within the confining slab-shaped cavity as trapped in an infinite potential well in the z-direction, the quantization of the wave vector $k_z(n) = \pi n/D$ limits the allowed values of the A-phase energy gap to [59]

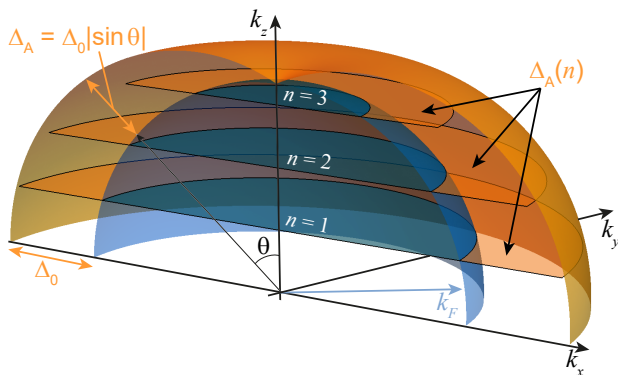$$\Delta_A(n) = \Delta_0\sqrt{1 - \frac{n^2}{n_0^2}}. \qquad (4)$$

FIG. 4. (Color online) Illustration of the allowed substates of the Fermi sphere and the A-phase energy gap resulting from the quantization of k_z in a very thin film of superfluid ^{3}He. The *blue quarter sphere* represents part of the Fermi sphere with radius k_F. The *orange surface* around it is a schematic illustration of the bulk A-phase energy gap $\Delta_A = \Delta_0|\sin\theta|$, where θ is the angle between the anisotropy axis $\hat{\mathbf{l}} \parallel \hat{\mathbf{z}}$ and $\hat{\mathbf{k}}$ [35]. The allowed substates of k_z due to the size quantization are drawn as disks labeled by n. In this example the maximum number of substates of k_z below k_F is 3, and the highest substate does not coincide with the node in the gap, i.e., $3 < n_0 < 4$. The energy gap $\Delta_A(n)$ corresponding to each disk follows from Eq. (4). The gap and the Fermi sphere are not drawn to scale since $\Delta_0 \ll E_F$, where E_F is the Fermi energy.

Here $n \leq n_0$ is an integer and $n_0 = k_F D/\pi$, which generally is not an integer, is the maximum available number of Fermi disks for $0 < k_z \leq k_F$, where $k_z(n_0) = k_F$ at the pole of the Fermi surface. By fine tuning the system by adjusting the quantization condition to align the largest allowed k_z away from k_F, one could eliminate nodes entirely from the energy gap, see Fig. 4. In our $D = 80$ nm cavity $n_0 \approx 200$, which sets the Fermi disks too densely to see any quantization effects within the temperature range covered by us. However, taking for example a $D = 10$ nm cavity, where $n_0 \approx 25$, the minimum value of the gap corresponding to the largest available k_z could be as high as $0.28\Delta_0$ [59]. Such a fully-gapped chiral superfluid at very low—but achievable—temperatures, without the usual node-bound thermal quasiparticle excitations present, enables access to the physics of the two-dimensional superfluid film [34]. We also note that as the normal state becomes progressively more 2D within more confined systems, the Fermi liquid properties and spin-fluctuation pairing interactions may be modified, and eventually impact the stability of the 2D ^{3}He-A as well. Until that limit the quantization of k_z should enhance the quest to detect the emergent chiral-specific phenomena, such as the quantum Hall effect [2, 5] and the edge-bound chiral Majorana-Weyl states and the corresponding ground-state edge currents. In addition, confining such a thin ^{3}He-A film laterally has been predicted to lead to a sequence of phase transitions into a pair-density-wave phase and the polar phase [74].

———

* Contact author: petri.heikkinen@rhul.ac.uk
† Current address: Department of Physics, University of Oxford, Oxford OX1 3PU, United Kingdom
‡ Contact author: j.saunders@rhul.ac.uk
§ Current address: Department of Physics, University of Oregon, Eugene, Oregon 97403, USA
¶ Current address: VTT Technical Research Centre of Finland Ltd, Espoo 02150, Finland

[1] C. Kallin and J. Berlinsky, Chiral superconductors, Reports on Progress in Physics **79**, 054502 (2016).
[2] G. E. Volovik, Quantum Hall state and chiral edge state in thin ^{3}He-A film, JETP Letters **55**, 368 (1992).
[3] T. Kita, Angular momentum of anisotropic superfluids at finite temperatures, Journal of the Physical Society of Japan **67**, 216 (1998).
[4] M. Stone and R. Roy, Edge modes, edge currents, and gauge invariance in $p_x + ip_y$ superfluids and superconductors, Physical Review B **69**, 184511 (2004).
[5] G. E. Volovik, An analog of the quantum Hall effect in a superfluid ^{3}He film, Sov. Phys. JETP **67**, 1804 (1988).
[6] N. Read and D. Green, Paired states of fermions in two dimensions with breaking of parity and time-reversal symmetries and the fractional quantum Hall effect, Physical Review B **61**, 10267 (2000).
[7] G. E. Volovik and V. P. Mineev, Line and point singularities in superfluid ^{3}He, JETP Letters **24**, 561 (1976).
[8] M. M. Salomaa and G. E. Volovik, Half-quantum vortices in superfluid ^{3}He-A, Physical Review Letters **55**, 1184 (1985).
[9] G. E. Volovik, Monopole, half-quantum vortex, and nexus in chiral superfluids and superconductors, JETP Letters **70**, 792 (1999).
[10] D. A. Ivanov, Non-Abelian statistics of half-quantum vortices in p-wave superconductors, Physical Review Letters

86, 268 (2001).

[11] J. A. Sauls, Surface states, edge currents, and the angular momentum of chiral p-wave superfluids, Physical Review B **84**, 214509 (2011).

[12] G. Moore and N. Read, Nonabelions in the fractional quantum Hall effect, Nuclear Physics B **360**, 362 (1991).

[13] G. E. Volovik, Fermion zero modes on vortices in chiral superconductors, JETP Letters **70**, 609 (1999).

[14] A. P. Schnyder, S. Ryu, A. Furusaki, and A. W. W. Ludwig, Classification of topological insulators and superconductors in three spatial dimensions, Physical Review B **78**, 195125 (2008).

[15] M. Sato and Y. Ando, Topological superconductors: a review, Reports on Progress in Physics **80**, 076501 (2017).

[16] A. Yu. Kitaev, Fault-tolerant quantum computation by anyons, Annals of Physics **303**, 2 (2003).

[17] C. W. J. Beenakker, Search for Majorana fermions in superconductors, Annu. Rev. Condens. Matter Phys. **4**, 113 (2013).

[18] S. Das Sarma, M. Freedman, and C. Nayak, Majorana zero modes and topological quantum computation, npj Quantum Information **1**, 1 (2015).

[19] B. Lian, X.-Q. Sun, A. Vaezi, X.-L. Qi, and S.-C. Zhang, Topological quantum computation based on chiral Majorana fermions, Proceedings of the National Academy of Sciences **115**, 10938 (2018).

[20] S. K. Ghosh, M. Smidman, T. Shang, J. F. Annett, A. D. Hillier, J. Quintanilla, and H. Yuan, Recent progress on superconductors with time-reversal symmetry breaking, Journal of Physics: Condensed Matter **33**, 033001 (2020).

[21] A. Ramires, Symmetry aspects of chiral superconductors, Contemporary Physics **63**, 71 (2022).

[22] A. Pustogow, Y. Luo, A. Chronister, Y.-S. Su, D. A. Sokolov, F. Jerzembeck, A. P. Mackenzie, C. W. Hicks, N. Kikugawa, S. Raghu, E. D. Bauer, and S. E. Brown, Constraints on the superconducting order parameter in Sr_2RuO_4 from oxygen-17 nuclear magnetic resonance, Nature **574**, 72 (2019).

[23] H. G. Suh, H. Menke, P. M. R. Brydon, C. Timm, A. Ramires, and D. F. Agterberg, Stabilizing even-parity chiral superconductivity in Sr_2RuO_4, Physical Review Research **2**, 032023(R) (2020).

[24] V. Grinenko, D. Das, R. Gupta, B. Zinkl, N. Kikugawa, Y. Maeno, C. W. Hicks, H.-H. Klauss, M. Sigrist, and R. Khasanov, Unsplit superconducting and time reversal symmetry breaking transitions in Sr_2RuO_4 under hydrostatic pressure and disorder, Nature Communications **12**, 3920 (2021).

[25] R. Joynt and L. Taillefer, The superconducting phases of UPt_3, Reviews of Modern Physics **74**, 235 (2002).

[26] J. D. Strand, D. J. Van Harlingen, J. B. Kycia, and W. P. Halperin, Evidence for complex superconducting order parameter symmetry in the low-temperature phase of UPt_3 from Josephson interferometry, Physical Review Letters **103**, 197002 (2009).

[27] E. R. Schemm, W. J. Gannon, C. M. Wishne, W. P. Halperin, and A. Kapitulnik, Observation of broken time-reversal symmetry in the heavy-fermion superconductor UPt_3, Science **345**, 190 (2014).

[28] K. E. Avers, W. J. Gannon, S. J. Kuhn, W. P. Halperin, J. A. Sauls, L. DeBeer-Schmitt, C. D. Dewhurst, J. Gavilano, G. Nagy, U. Gasser, and M. R. Eskildsen, Broken time-reversal symmetry in the topological superconductor UPt_3, Nature Physics **16**, 531 (2020).

[29] L. Jiao, S. Howard, S. Ran, Z. Wang, J. O. Rodriguez, M. Sigrist, Z. Wang, N. P. Butch, and V. Madhavan, Chiral superconductivity in heavy-fermion metal UTe_2, Nature **579**, 523 (2020).

[30] P. K. Biswas, S. K. Ghosh, J. Z. Zhao, D. A. Mayoh, N. D. Zhigadlo, X. Xu, C. Baines, A. D. Hillier, G. Balakrishnan, and M. R. Lees, Chiral singlet superconductivity in the weakly correlated metal $LaPt_3P$, Nature Communications **12**, 2504 (2021).

[31] P. K. Biswas, H. Luetkens, T. Neupert, T. Stürzer, C. Baines, G. Pascua, A. P. Schnyder, M. H. Fischer, J. Goryo, M. R. Lees, H. Maeter, F. Brückner, H.-H. Klauss, M. Nicklas, P. J. Baker, A. D. Hillier, M. Sigrist, A. Amato, and D. Johrendt, Evidence for superconductivity with broken time-reversal symmetry in locally noncentrosymmetric SrPtAs, Physical Review B **87**, 180503(R) (2013).

[32] M. H. Fischer, T. Neupert, C. Platt, A. P. Schnyder, W. Hanke, J. Goryo, R. Thomale, and M. Sigrist, Chiral d-wave superconductivity in SrPtAs, Physical Review B **89**, 020509(R) (2014).

[33] J. A. Mydosh, P. M. Oppeneer, and P. Riseborough, Hidden order and beyond: an experimental—theoretical overview of the multifaceted behavior of URu_2Si_2, Journal of Physics: Condensed Matter **32**, 143002 (2020).

[34] G. E. Volovik, *Exotic properties of superfluid helium 3*, Series in Modern Condensed Matter Physics, Vol. 1 (World Scientific, 1992).

[35] D. Vollhardt and P. Wölfle, *The superfluid phases of helium 3*, dover ed. (Dover Publications, New York, 2013).

[36] G. E. Volovik, *The Universe in a helium droplet*, International Series of Monographs on Physics, Vol. 117 (Oxford University Press, Oxford, 2003).

[37] P. M. Walmsley and A. I. Golov, Chirality of superfluid ^{3}He-A, Physical Review Letters **109**, 215301 (2012).

[38] H. Ikegami, Y. Tsutsumi, and K. Kono, Chiral symmetry breaking in superfluid ^{3}He-A, Science **341**, 59 (2013).

[39] H. Ikegami, Y. Tsutsumi, and K. Kono, Observation of intrinsic magnus force and direct detection of chirality in superfluid ^{3}He-A, Journal of the Physical Society of Japan **84**, 044602 (2015).

[40] J. Kasai, Y. Okamoto, K. Nishioka, T. Takagi, and Y. Sasaki, Chiral domain structure in superfluid ^{3}He-A studied by magnetic resonance imaging, Physical Review Letters **120**, 205301 (2018).

[41] T. Mizushima, Y. Tsutsumi, M. Sato, and K. Machida, Symmetry protected topological superfluid ^{3}He-B, Journal of Physics: Condensed Matter **27**, 113203 (2015).

[42] A. L. Fetter and S. Ullah, Superfluid density and critical current of ^{3}He in confined geometries, Journal of Low Temperature Physics **70**, 515 (1988).

[43] M. R. Freeman, R. S. Germain, E. V. Thuneberg, and R. C. Richardson, Size effects in thin films of superfluid ^{3}He, Physical Review Letters **60**, 596 (1988).

[44] Y. Nagato and K. Nagai, A–B transition of superfluid ^{3}He in a slab with rough surfaces, Physica B: Condensed Matter **284**, 269 (2000).

[45] A. B. Vorontsov and J. A. Sauls, Thermodynamic properties of thin films of superfluid ^{3}He-A, Physical Review B **68**, 064508 (2003).

[46] L. V. Levitin, R. G. Bennett, A. Casey, B. Cowan, J. Saunders, D. Drung, Th. Schurig, and J. M. Parpia, Phase diagram of the topological superfluid ^{3}He confined in a nanoscale slab geometry, Science **340**, 841 (2013).

[47] P. J. Heikkinen, A. Casey, L. V. Levitin, X. Rojas, A. Vorontsov, P. Sharma, N. Zhelev, J. M. Parpia, and J. Saunders, Fragility of surface states in topological superfluid ^{3}He, Nature Communications **12**, 1574 (2021).

[48] V. Ambegaokar, P. G. deGennes, and D. Rainer, Landau-Ginsburg equations for an anisotropic superfluid, Physical Review A **9**, 2676 (1974).

[49] L. H. Kjäldman, J. Kurkijärvi, and D. Rainer, Suppression of P-wave superfluidity in long, narrow pores, Journal of Low Temperature Physics **33**, 577 (1978).

[50] Y. Nagato, M. Yamamoto, and K. Nagai, Rough surface effects on the p-wave Fermi superfluids, Journal of Low Temperature Physics **110**, 1135 (1998).

[51] A. B. Vorontsov, Andreev bound states in superconducting films and confined superfluid ^{3}He, Philosophical Transactions of the Royal Society A: Mathematical, Physical and Engineering Sciences **376**, 20150144 (2018).

[52] J. Xu and B. C. Crooker, Very thin films of ^{3}He: a new phase?, Physical Review Letters **65**, 3005 (1990).

[53] L. V. Levitin, R. G. Bennett, A. Casey, B. P. Cowan, C. P. Lusher, J. Saunders, D. Drung, and Th. Schurig, A nuclear magnetic resonance spectrometer for operation around 1 MHz with a sub-10-mK noise temperature, based on a two-stage dc superconducting quantum interference device sensor, Applied Physics Letters **91**, 262507 (2007).

[54] P. J. Heikkinen, N. Eng, L. V. Levitin, X. Rojas, A. Singh, S. Autti, R. P. Haley, M. Hindmarsh, D. E. Zmeev, J. M. Parpia, A. Casey, and J. Saunders, Nanofluidic platform for studying the first-order phase transitions in superfluid helium-3, Journal of Low Temperature Physics **215**, 477 (2024).

[55] S. Dimov, R. G. Bennett, A. Córcoles, L. V. Levitin, B. Ilic, S. S. Verbridge, J. Saunders, A. Casey, and J. M. Parpia, Anodically bonded submicron microfluidic chambers, Review of Scientific Instruments **81**, 013907 (2010).

[56] N. Zhelev, T. S. Abhilash, R. G. Bennett, E. N. Smith, B. Ilic, J. M. Parpia, L. V. Levitin, X. Rojas, A. Casey, and J. Saunders, Fabrication of microfluidic cavities using Si-to-glass anodic bonding, Review of Scientific Instruments **89**, 073902 (2018).

[57] R. S. Bonilla, B. Hoex, P. Hamer, and P. R. Wilshaw, Dielectric surface passivation for silicon solar cells: A review, Physica Status Solidi A **214**, 1700293 (2017).

[58] R. Kotipalli, R. Delamare, O. Poncelet, X. Tang, L. A. Francis, and D. Flandre, Passivation effects of atomic-layer-deposited aluminum oxide, EPJ Photovoltaics **4**, 45107 (2013).

[59] See Supplemental Material at [URL will be inserted by publisher] for the near-specular gap suppression, discussion on initial slopes, derivation of the strong-coupling model, ruling out the planar phase, and derivation of the size quantization of the energy gap.

[60] M. R. Rand, *Nonlinear spin dynamics and magnetic field distortion of the superfluid ^{3}He-B order parameter*, Ph.D. thesis, Northwestern University (1996).

[61] M. R. Rand, H. H. Hensley, J. B. Kycia, T. M. Haard, Y. Lee, P. J. Hamot, and W. P. Halperin, New NMR evidence: can an axi-planar superfluid ^{3}He-A order parameter be ruled out?, Physica B **194-196**, 805 (1994).

[62] A. M. Zimmerman, M. D. Nguyen, and W. P. Halperin, NMR frequency shifts and phase identification in superfluid ^{3}He, Journal of Low Temperature Physics **195**, 358 (2019).

[63] P. Schiffer, M. T. O'Keefe, H. Fukuyama, and D. D. Osheroff, Low-temperature studies of the NMR frequency shift in superfluid ^{3}He-A, Physical review letters **69**, 3096 (1992).

[64] A. I. Ahonen, M. Krusius, and M. A. Paalanen, NMR experiments on the superfluid phases of ^{3}He in restricted geometries, Journal of Low Temperature Physics **25**, 421 (1976).

[65] L. V. Levitin, R. G. Bennett, E. V. Surovtsev, J. M. Parpia, B. Cowan, A. J. Casey, and J. Saunders, Surface-induced order parameter distortion in superfluid ^{3}He-B measured by nonlinear NMR, Physical Review Letters **111**, 235304 (2013).

[66] L. V. Levitin, B. Yager, L. Sumner, B. Cowan, A. J. Casey, J. Saunders, N. Zhelev, R. G. Bennett, and J. M. Parpia, Evidence for a spatially modulated superfluid phase of ^{3}He under confinement, Physical Review Letters **122**, 085301 (2019).

[67] D. S. Greywall, ^{3}He specific heat and thermometry at millikelvin temperatures, Physical Review B **33**, 7520 (1986).

[68] M. R. Freeman and R. C. Richardson, Size effects in superfluid ^{3}He films, Physical Review B **41**, 11011 (1990).

[69] S. M. Tholen and J. M. Parpia, Slip and the effect of ^{4}He at the ^{3}He-silicon interface, Physical Review Letters **67**, 334 (1991).

[70] J. W. Serene and D. Rainer, The quasiclassical approach to superfluid ^{3}He, Physics Reports **101**, 221 (1983).

[71] H. Choi, J. P. Davis, J. Pollanen, T. M. Haard, and W. P. Halperin, Strong coupling corrections to the Ginzburg-Landau theory of superfluid ^{3}He, Physical Review B **75**, 174503 (2007).

[72] J. J. Wiman and J. A. Sauls, Superfluid phases of ^{3}He in nanoscale channels, Physical Review B **92**, 144515 (2015).

[73] J. Saunders, Realizing quantum materials with helium: helium films at ultralow temperatures, from strongly correlated atomically layered films to topological superfluidity, in *Topological Phase Transitions and New Developments*, edited by L. Brink, M. Gunn, J. V. José, J. M. Kosterlitz, and K. K. Phua (World Scientific Publishing, Singapore, 2019) pp. 165–196, https://arxiv.org/abs/1910.01058.

[74] H. Wu and J. A. Sauls, Weyl Fermions and broken symmetry phases of laterally confined ^{3}He films, Journal of Physics: Condensed Matter **35**, 495402 (2023).

[75] P. J. Heikkinen, L. V. Levitin, X. Rojas, A. Singh, N. Eng, A. Vorontsov, N. Zhelev, T. S. Abhilash, J. M. Parpia, A. Casey, and J. Saunders, Accompanying data for "Chiral superfluidity of helium-3 in the quasi-two-dimensional limit" (2024), Figshare, https://doi.org/10.17637/rh.27020611.

Chiral superfluidity of helium-3 in the quasi-two-dimensional limit: Supplemental Material

Petri J. Heikkinen,* Lev V. Levitin, Xavier Rojas, Angadjit Singh,† Nathan Eng, Andrew Casey, and John Saunders‡

Department of Physics, Royal Holloway, University of London, Egham TW20 0EX, Surrey, United Kingdom

Anton Vorontsov

Department of Physics, Montana State University, Bozeman, Montana 59717, USA

Nikolay Zhelev,§ Abhilash Thanniyil Sebastian,¶ and Jeevak M. Parpia

Department of Physics, Cornell University, Ithaca, New York 14853, USA

(Dated: September 20, 2024)

GAP SUPPRESSION BY SPECULARITY $S = 0.98$

Any non-specular boundary condition ($S < 1.0$) spatially suppresses the energy gap close to the surfaces, resulting in the suppression of the superfluid transition temperature T_c [45, 50]. Despite the acquired spatial dependence of the gap, the NMR precession within a confinement $D \ll \xi_D$ is uniform. Here $\xi_D \sim 10\,\mu$m is the dipolar length [35]. Frequency shift Δf is determined by the spatially averaged value of the squared energy gap, $\langle \Delta_0^2(z) \rangle$, and Eq. (1) in the main text can be written as [46, 47]

$$\langle \Delta_0^2(z) \rangle = \frac{\mathrm{IS}_\Delta}{\mathrm{IS}_f} \left| f^2 - f_L^2 \right|. \qquad (S1)$$

The T_c-suppression measurements presented in Fig. 1c in the main text give surface specularity close to $S = 0.98$ within our $D = 80\,$nm cavity. The corresponding suppression of the energy gap, based on the calculations using the quasiclassical weak-coupling theory [45, 51, 70] and shown in Fig. S1a, is minuscule over the full pressure and temperature span, allowing the identification of the superfluid phase within the cavity as ^{3}He-A. Additionally, this cannot explain the observed deviation of the inferred gap values (Fig. 3 in the main text and Fig. S3 here) from the weak-coupling BCS (bulk ^{3}He-A, $S = 1.0$) temperature dependence, allowing the precise determination of the strong-coupling effects particularly visible at higher pressures. For example, at 21.0 bar the calculated squared energy gap with $S = 0.98$ deviates from the squared BCS gap only by less than 1% over the full temperature range, see Fig. S1b.

INITIAL SLOPES

The initial slope $\mathrm{IS}_f = \partial \left| f^2 - f_L^2 \right| / \partial \left(1 - T/T_c \right)$ is a good indicator distinguishing between different superfluid phases. It can be determined from the linear fit for the squared precession frequency shift $\left| f^2 - f_L^2 \right|$ versus temperature [46, 47]. The agreement is truly linear only very close to T_c so the temperature range used
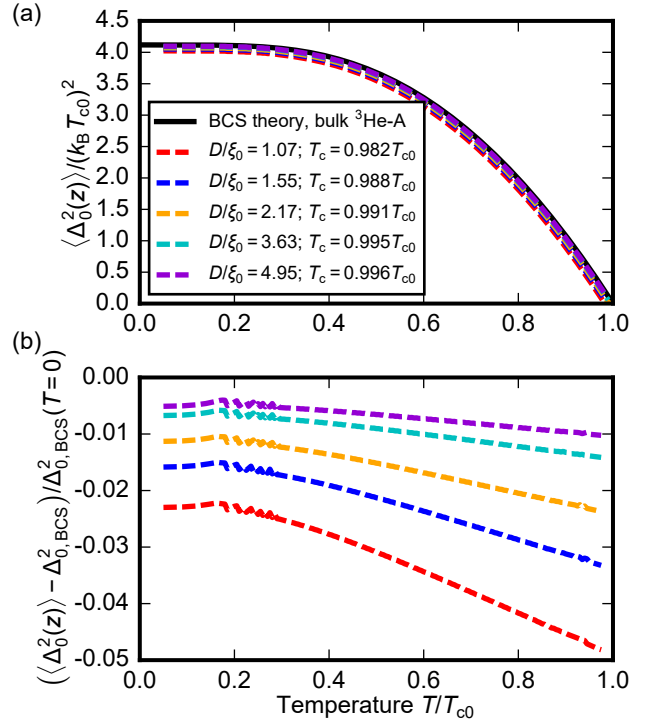

FIG. S1. (a) The spatially averaged values of the squared energy gap with specularity $S = 0.98$ corresponding to different effective cavity heights D/ξ_0 (*colored dashed lines*) do not significantly deviate from the BCS temperature dependence of the squared bulk ^{3}He-A gap, equivalent to $S = 1.0$ (*black solid line*). The used values of D/ξ_0 are consistent with pressures 0.2, 2.5, 5.5, 12.0, and 21.0 bar within a $D = 80\,$nm high cavity, from the lowest given value of D/ξ_0 to the highest, respectively, taking into account the cavity height distortion by pressure [47]. (b) The deviation of the calculated spatially averaged values from the squared BCS gap $\Delta_{0,\mathrm{BCS}}^2$ relative to its value at $T = 0$. The relative difference smoothly decreases with decreasing temperature, with the strongest confinement (the smallest D/ξ_0) showing the largest suppression. The lines do not reach up to T_{c0} due to small suppression of T_c, given in the legend in panel (a). The ripples visible around $T_c/T_{c0} \approx 0.2$ are artifacts from the calculations.
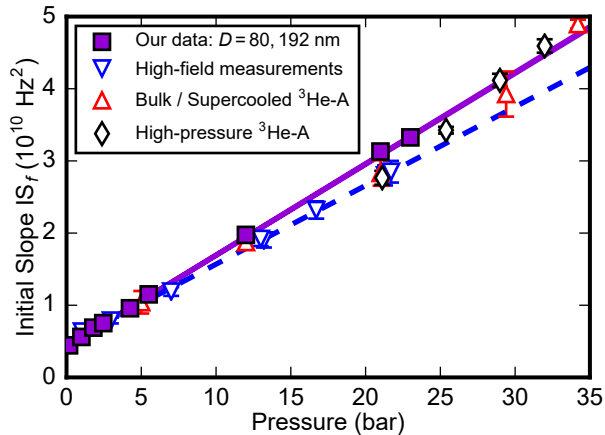
FIG. S2. Initial slopes of frequency shift versus temperature determined within range $0.95T_c < T < T_c$ compared to previous bulk ^{3}He-A experiments. *Violet squares* show the combined specular data from cavities with $D = 80\,\mathrm{nm}$ and $D = 192\,\mathrm{nm}$ [47]. *Violet line* is a linear fit to these data. The high-field experiments (*blue downward-pointing triangles*) and the linear fit (*the blue dashed line*) of the bulk ^{3}He-A initial slope are from Refs. [60–62] using the same 5% range below T_c for determining them. The data based on stable and/or supercooled bulk ^{3}He-A are from Ref. [63] (*red upward-pointing triangles*) and from Ref. [64] (*black diamonds*). In these works the used range differed from 5%, so the values have been adjusted to compensate for the systematic differences [47].

in the determination of the experimental value needs to be carefully chosen. In the main text we use range $0.90T_c < T < T_c$ which is a suitable compromise between precision and accuracy, taking into account the number of data points within the range and the related uncertainties [47]. Initial slope defined this way is thus ideal for the conversion between the measured frequency shift and the energy gap. However, various temperature ranges have been used to infer the values of the initial slope reported in the literature. To avoid the systematic differences and to allow comparison, we adjust the values using the relative range dependence of the initial slope of the calculated weak-coupling energy gap $\mathrm{IS}_\Delta^{\mathrm{BCS}} = \partial \Delta_{0,\mathrm{BCS}}^2 / \partial\left(1 - T/T_{c0}\right)$, as described in Ref. [47]. In Fig. S2 we show the data using range $0.95T_c < T < T_c$ to allow unadjusted comparison to the most complete data set from the earlier bulk ^{3}He-A experiments in Refs. [60–62]. We also combine the data measured with cavities of $D = 80\,\mathrm{nm}$ (this work) and $D = 192\,\mathrm{nm}$ [47] (data only available below $P \le 5.5\,\mathrm{bar}$) having similar ^{4}He preplating. The other included experiments used different ranges [63, 64], so we have used the abovementioned scaling to bring those values into the same 5% range below T_c. The value of IS_f increases linearly with pressure, as seen before, and our measurements are in a good agreement with the earlier work.

STRONG-COUPLING TEMPERATURE DEPENDENCE

Near the superfluid transition temperature T_{c0} the energy gap can be described by Ginzburg-Landau (G-L) theory and directly related to the specific-heat jump ΔC_A at the transition. In the A phase the maximum Δ_0 of the gap in momentum space is given by [35]

$$\Delta_0^2(T) = \frac{\alpha(T)}{4\beta_{245}} = \frac{\Delta C_A}{C_N}(\pi k_B T_{c0})^2(1 - T/T_{c0}), \quad (\mathrm{S2})$$

where $\alpha(T)$ and β_{245} are coefficients of the G-L theory. The full temperature dependence of the gap is well-established within the weak-coupling BCS theory. In this limit the scale of the gap, $\Delta_{0,\mathrm{BCS}}(T)$, is fully determined by the value of T_{c0}. However, since the experimentally observed $\Delta C_A \propto \beta_{245}^{-1}$ is larger than the BCS value [71], the gap is enhanced by the strong-coupling effects, the more the higher the pressure.

A simple way to take this into account, used in Ref. [47], is to scale $\Delta_{0,\mathrm{BCS}}(T)$ using the established behavior near T_{c0}:

$$\Delta_0^2(T) = \frac{\Delta C_A}{\Delta C_A^{\mathrm{BCS}}}\Delta_{0,\mathrm{BCS}}^2(T) = \frac{\beta_{245}^{\mathrm{BCS}}}{\beta_{245}}\Delta_{0,\mathrm{BCS}}^2(T). \quad (\mathrm{S3})$$

Eq. (S3) successfully describes the pressure-dependence of the straight-line behavior of $\Delta_0^2(T)$ in the G-L regime, Eq. (S2), but overshoots the data at lower temperatures, see Fig. S3 and Fig. 3 in the main text. This is a manifestation of the reduction of the strong coupling effects on cooling. Wiman and Sauls have suggested to incorporate this phenomenon into the G-L theory by giving all β_i coefficients a temperature dependence [72]

$$\delta\beta_i(T) \equiv \beta_i(T) - \beta_i^{\mathrm{BCS}} = \left(\beta_i(T_{c0}) - \beta_i^{\mathrm{BCS}}\right)\frac{T}{T_{c0}}$$
$$= \delta\beta_i(T_{c0})\frac{T}{T_{c0}}, \quad (\mathrm{S4})$$

where $\beta_i(T_{c0}) \equiv \beta_i$ is the conventional G-L parameter at T_{c0} based on a set of experiments [71]. In particular,

$$\frac{\delta\beta_{245}(T_{c0})}{\beta_{245}^{\mathrm{BCS}}} = \frac{\Delta C_A^{\mathrm{BCS}}}{\Delta C_A} - 1. \quad (\mathrm{S5})$$

Next we combine Eqs. (S3) and (S4):

$$\Delta_0^2(T) = \frac{\beta_{245}^{\mathrm{BCS}}}{\beta_{245}(T)}\Delta_{0,\mathrm{BCS}}^2(T)$$
$$= \frac{\Delta_{0,\mathrm{BCS}}^2(T)}{1 + \dfrac{\delta\beta_{245}(T_{c0})}{\beta_{245}^{\mathrm{BCS}}}\dfrac{T}{T_{c0}}}. \quad (\mathrm{S6})$$

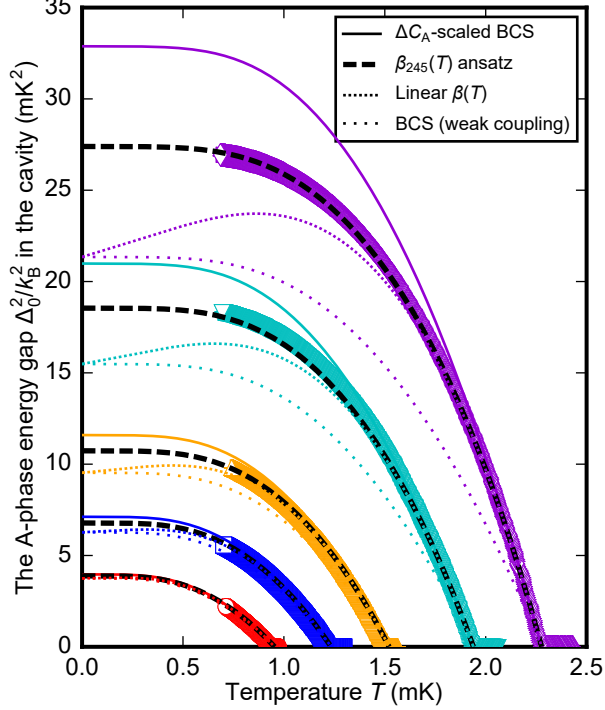This model improves the agreement with the NMR data down to $T \sim 0.7T_{c0}$, consistent with the key success

FIG. S3. Comparison of the measured and calculated energy gap. Calculations beyond the BCS T-dependence are based on Eqs. (S6) (*densely dotted lines*) and (S8) (*dashed lines*). The pressures from the lowest to the highest data set are 0.2, 2.5, 5.5, 12.0, and 21.0 bar, respectively.

of Eq. (S4) in capturing the bulk A-B phase boundary $T_{AB}(P)$ [72], which occurs above $\min(T_{AB}) = 0.78T_{c0}$. At lower temperatures Eq. (S6) underestimates the gap, with unphysical prediction that at any pressure the weak coupling limit is reached at $T \to 0$, see Fig. S3.

A very good agreement with the experimental data is obtained by replacing T/T_{c0} in Eq. (S4) with a function of temperature behaving similarly above $0.7T_{c0}$ but not dropping all the way to zero at $T \to 0$,

$$\delta\beta_i(T) = \delta\beta_i(T_{c0})\left(1 - 0.09\frac{\Delta_{0,\mathrm{BCS}}^2(T)}{k_\mathrm{B}^2 T_{c0}^2}\right). \qquad \text{(S7)}$$

This expression, illustrated in Fig. S3 and also in Fig. 3 in the main text, leads to a successful ansatz for the temperature dependence of the energy gap:

$$\begin{aligned}\Delta_0^2(T) &= \frac{\beta_{245}^{\mathrm{BCS}}}{\beta_{245}(T)}\Delta_{0,\mathrm{BCS}}^2(T) \qquad \text{(S8)}\\[2mm] &= \frac{\Delta_{0,\mathrm{BCS}}^2(T)}{1 + \dfrac{\delta\beta_{245}(T_{c0})}{\beta_{245}^{\mathrm{BCS}}}\left(1 - 0.09\dfrac{\Delta_{0,\mathrm{BCS}}^2(T)}{k_\mathrm{B}^2 T_{c0}^2}\right)}.\end{aligned}$$

Here the factor 0.09 is chosen to roughly fit the data. Since a similar expression with a freely chosen prefac-

tor could be constructed using the B-phase gap, it remains as a task for the future to test whether Eqs. (S7) and (S8) based on the relevant weak-coupling gap values could quantitatively describe also the B phase or distorted phases under confinement.
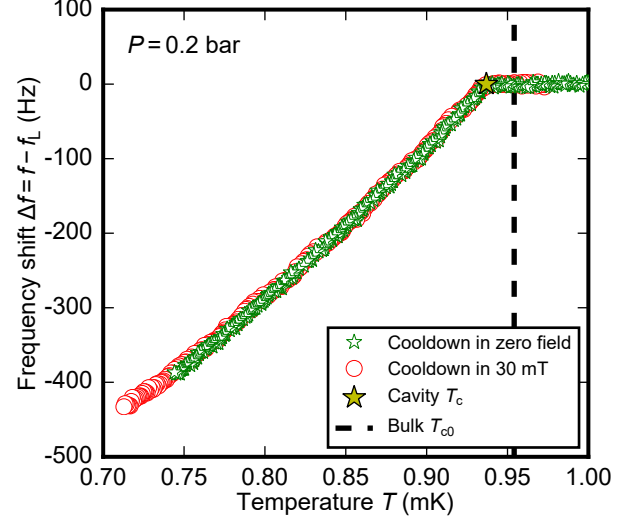
METASTABLE PLANAR PHASE

FIG. S4. The superfluid frequency shift in the $D = 80\,\mathrm{nm}$ cavity at 0.2 bar during a temperature sweep up after first cooling down through T_c with the NMR field off (*green stars*) vs. the usual NMR field on at $H_0 \approx 30\,\mathrm{mT}$ (*red circles*). Since in both cases Δf is negative and identical, the planar phase is ruled out as a possibility. Superfluid transition temperature T_c in the cavity is indicated by the *yellow star* and T_{c0} in the bulk marker by the *black dashed line*.

The A-phase order parameter in our experimental configuration ($\hat{\mathbf{d}} \perp \hat{\mathbf{z}}$ and $\hat{\mathbf{l}} \parallel \hat{\mathbf{z}}$) is written as [46]

$$\boldsymbol{\Delta}(\hat{\mathbf{p}}) = \Delta_0 (\hat{p}_x + i\hat{p}_y) \left[|\uparrow\uparrow\rangle + |\downarrow\downarrow\rangle\right]. \qquad \text{(S9)}$$

This form corresponds to $\hat{\mathbf{l}} = +\hat{\mathbf{z}}$ and is degenerate with order parameter of the form $\hat{p}_x - i\hat{p}_y$ corresponding to $\hat{\mathbf{l}} = -\hat{\mathbf{z}}$. The time-reversal invariant planar phase, which has not been observed experimentally, has a long-range order in the relative spin-orbit rotation and is degenerate with the A phase in the weak-coupling limit. Its order parameter is

$$\boldsymbol{\Delta}(\hat{\mathbf{p}}) = \Delta_0' (-\hat{p}_x + i\hat{p}_y) |\uparrow\uparrow\rangle + \Delta_0' (\hat{p}_x + i\hat{p}_y) |\downarrow\downarrow\rangle. \text{ (S10)}$$

In the weak-coupling limit these two phases have an identical energy gap, $\Delta_0 = \Delta_0'$.

In its minimum-energy state P_+, the planar phase would have a positive frequency shift. However, just like the B phase, the planar phase (which is the extreme

limit of the B phase with planar distortion) can exist in a metastable dipole-energy state P_- supported by the confinement and magnetic field [46, 65, 66]. This state would have identical NMR signatures with the dipole-unlocked A phase in the confining cavity: temperature-independent magnetization, negative frequency shift, and the same tipping-angle dependence. In the weak-coupling limit, especially relevant at low pressures, the magnitudes of the frequency shift would coincide as well, making the phase identification based on NMR signatures alone challenging.

We never observed positive frequency shift arising from the cavity, so P_+ phase is out of the question. Since in normal operation we always had the polarizing $H_0 \approx 30\,$mT NMR field on, it was possible, however unlikely, to stabilize the P_- phase within the cavity each time we cooled down into the superfluid state. Such a metastable phase could not exist without a magnetic field and instead converts to P_+ at fields below the dipole field $H_D \sim 3\,$mT [65]. Thus, we ruled it out by cooling through T_c in zero field at $P = 0.2\,$bar. After reaching $T \approx 0.75\,$mK, we ramped the field slowly back up before starting to record the NMR signals and to sweep the temperature up to characterize the superfluid frequency shift. Positive frequency shift at this point would have indicated an existence of a stable planar phase P_+. However, since Δf remained unchanged compared to the usual cooldowns (see Fig. S4), we confirmed that the dipole-unlocked A phase was stable even here.

A-PHASE GAP SIZE QUANTIZATION

In very thin superfluid films the size quantization in the momentum space results in the Fermi sphere transitioning into a series of Fermi disks, see illustration in Fig. 4 in the main text. In such a state only the energy gap values corresponding to the allowed momentum values are present, giving a possibility to avoid, e.g., any gap nodes existing in the full bulk energy gap. In the derivation below we do not consider any possible modifications to the pairing interactions by strong confinement.

The bulk A-phase energy gap is $\Delta_A = \Delta_0 |\sin\theta|$ where θ is the angle in momentum space between the anisotropy axis $\hat{\mathbf{l}}$ and $\hat{\mathbf{p}}$ [35]. Assuming for simplicity that the superfluid film in z-direction is trapped within an infinite potential well of width D, we get the set of allowed substates $k_z(n) = \pi n/D$ where n is an integer. If we take n_0 to be the total number of Fermi disks for $0 < k_z \leq k_F$ and assume that the substate corresponding to n_0 crosses the pole, where $\theta = 0$ and $\Delta_A = 0$, we have $k_z(n_0) = k_F$ and $n_0 = k_F D/\pi$. The value of k at the Fermi surface is $k_F = 7.9\,$nm^{-1} at $0\,$bar and $8.9\,$nm^{-1} at $34\,$bar.

We can write anywhere on the Fermi sphere (we assume $0 \leq \theta \leq \pi/2$, the rest follows from the symmetry)

$$\cos\theta = \frac{k_z}{k_F} \Rightarrow \sin\theta = \sqrt{1 - \frac{k_z^2}{k_F^2}}. \qquad \text{(S11)}$$

This allows us to write the A-phase energy gap as a function of n:

$$\Delta_A(n) = \Delta_0 \sin\theta = \Delta_0 \sqrt{1 - \frac{n^2}{n_0^2}}. \qquad \text{(S12)}$$

If one fine tunes the above system, e.g., by adjusting P and/or D, to push the allowed values of k_z up, thus making n_0 non-integer, the nodes in the gap and the related low-energy states for the quasiparticles disappear [5]. As a result, the energy gap corresponding to the highest substate $n < n_0$ becomes the smallest allowed gap value, $\min(\Delta_A)$.

The larger $\min(\Delta_A)$ is the easier it is to cool the system down to temperatures where the gaplessness of chiral ^{3}He-A is fully manifested and the physics of two-dimensional film can be accessed [34]. For example, taking $D = 10\,$nm and $P = 0\,$bar, we would have $n_0 \approx 25$ and $\min(\Delta_A) \approx 0.28\Delta_0$. The corresponding temperatures in ^{3}He are accessible.